HHS Public Access

Author manuscript

Prostate. Author manuscript; available in PMC 2020 January 11.

Development of an orthotopic canine prostate cancer model expressing human GRPr

Michael F. Tweedle, PhD[1], **Haiming Ding, PhD**[1], **William T. Drost, DVM**[2], **Joshua Dowell, MD, PhD**[1], **James Spain, MD, PhD**[1], **Mathew Joseph, BS**[3], **Said M. Elshafae, PhD**[1], **Maria-Isabela Menendez, DVM, PhD**[1], **Li Gong, PhD**[1], **Shankaran Kothandaraman, PhD**[1], **Wessel P. Dirksen, PhD**[4], **Chadwick L. Wright, MD, PhD**[1], **Robert Bahnson, MD**[5], **Michael V. Knopp, MD, PhD**[1], and **Thomas J. Rosol, MD, PhD**[6]

[1]Deptartment of Radiology, The Wright Center for Innovation in Biomolecular Imaging, The Ohio State University, Columbus, Ohio

[2]Deptartment of Veterinary Clinical Sciences, The Ohio State University, Columbus, Ohio

[3]University Laboratory Animal Resources, The Ohio State University, Columbus, Ohio

[4]Deptartment of Veterinary Biosciences, The Ohio State University, Columbus, Ohio

[5]Deptartment of Urology, Wexner Medical Center, The Ohio State University, Columbus, Ohio

[6]Deptartment of Biomedical Sciences, Ohio University, Athens, Ohio

Abstract

Background: Ace-1 canine prostate cancer cells grow orthotopically in cyclosporine immunosuppressed laboratory beagles. We previously transfected (human Gastrin-Releasing Peptide Receptor, huGRPr) into Ace-1 cells and demonstrated receptor-targeted NIRF imaging with IR800-G-Abz4-t-BBN, an agonist to huGRPr. Herein, we used the new cell line to develop the first canine prostate cancer model expressing a human growth factor receptor.

Methods: Dogs were immunosuppressed with cyclosporine, azathioprine, prednisolone, and methylprednisolone. Their prostate glands were implanted with Ace-1^{huGRPr} cells. The implantation wounds were sealed with a cyanoacrylic adhesive to prevent extraprostatic tumor growth. Intraprostatic tumors grew in 4–5 week. A lobar prostatic artery was then catheterized via the carotid artery and 25–100 nmol IR800-Abz4-t-BBN was infused in 2 mL followed by euthanasia in dogs 1–2, and recovery for 24 h before euthanasia in dogs 3–6. Excised tissues were imaged optically imaged, and histopathology performed.

Results: Dog1 grew no tumors with cyclosporine alone. Using the four drug protocol, Dogs 2–6 grew abundant 1–2 mm intracapsular and 1–2 cm intraglandular tumors. Tumors grew >5 cm when the prostate cancer cells became extracapsular. Dogs 4–6 with sealed prostatic capsule implantation sites had growth of intracapsular and intraglandular tumors and LN metastases at 5

Correspondence Michael F. Tweedle, PhD, Department of Radiology, The Ohio State University, Columbus, OH 43210. michael.tweedle@osumc.edu.

CONFLICTS OF INTEREST

All authors have no conflicts of interest in this work.

weeks. High tumor to background BPH signal in the NIRF images of sectioned prostate glands resulted from the 100 nmol dose (~8 nmol/kg) in dogs 2–4 and 50 nmol dose in dog 5, but not from the 25 nmol dose in Dog 6. Imaging of mouse Ace-1^{huGRPr} tumors required an intravenous dose of 500 nmol/kg body wt. A lymph node that drained the prostate gland was detectable in Dog 4. Histologic findings confirmed the imaging data.

Conclusion: Ace-1^{huGRPr} cells created viable, huGRPr-expressing tumors when implanted orthotopically into immune-suppressed dogs. Local delivery of an imaging agent through the prostatic artery allowed a very low imaging dose, suggesting that therapeutic agents could be used safely for treatment of early localized intraglandular prostate cancer as adjuvant therapy for active surveillance or focal ablation therapies, or for treating multifocal intraglandular disease where focal ablation therapies are not indicated or ineffective.

Keywords

bombesin; canine prostate cancer; GRP

1 | INTRODUCTION

Most of the over 200 000 prostate cancers diagnosed annually in the USA are treated by whole gland resection or ablation, a procedure accompanied by the significant side effects of impotence and incontinence. Advances in diagnostic tools, such as cancer specific biomarkers, MRI, and ultrasound (US) imaging have recently allowed for more accurate tumor grade and location,[1–3] and enabled Active Surveillance (AS) to become a clinically proven alternative to spare the prostate gland. But AS is currently limited to a small subset of patients with low risk disease, and/or the shortest life expectancy.[4,5] The subset of patients offered AS could be broadened by application of effective adjuvant anticancer therapies. However, cancer-specific pharmaceuticals are systemically delivered, usually in multiple repeat doses that inevitably generate strong off-target toxicity. Beam radiotherapy can be locally and regionally delivered but also generates significant off-target effects in the pelvic region due to radio sensitivity of the adjacent bladder and colon,[6] and there remains no accurate method to locate and irradiate only the tumor. To eliminate or acceptably reduce off-target effects in gland-sparing therapy, we are developing an intra-arterial drug delivery method that will use the proven clinical accessibility of the prostatic arteries and the large mass ratio of the prostate gland to the total body mass (25 g prostate vs 70 000 g body) to generate a high enough therapeutic index to enable adjuvant therapy in AS.

Arterial delivery of embolization beads is a well-documented procedure in the treatment of accessible metastases.[7] Radiolabeled embolization beads and drug-eluting embolization beads have been delivered in the setting of metastatic liver disease.[8] In prostate disease, arterial embolization has been tested successfully in hundreds of patients to relieve the symptoms of severe benign prostatic hypertrophy.[9,10] However, no attempts have been made in either animals or humans to deliver anticancer drugs to the prostate gland by this route.

Testing therapeutic agents delivered arterially to the prostate will require a large animal model. A canine model has been developed that uses cultured Ace-1 canine prostate cancer cells implanted into prostate glands of immune-suppressed beagles.[11] We previously

reported development of a novel Ace-1 cell line that was transfected with the human (hu) gastrin-releasing peptide receptor (GRPr) gene, producing a highly GRPr expressing and biologically functioning cell line, Ace-1^{huGRPr}, that grows stably in culture and in nude mice.[12,13] Nude mice xenografts were imaged with a 10 nmol intravenous dose of a GRPr-targeted optical imaging agent, IR800-G-Abz4-AMBA.[14] Herein we report the successful translation of these developments to dogs. We have developed an orthotopic canine prostate cancer model that expresses human GRPr and can be imaged with near infrared fluorescent (NIRF) optical imaging after transcatheter arterial delivery of only 50 nmol of IR800-G-Abz4-AMBA. We believe this is the first demonstration of a human cancer growth factor receptor that has been expressed and imaged in a canine model.

2 | MATERIALS AND METHODS

2.1 | Ethics statement

All animal experiments were conducted according to NIH guidelines, and according to protocols approved by the Institutional Animal Care and Use Committee of The Ohio State University.

2.2 | Previously described methods

We recently published descriptions of methods used to create and maintain the Ace-1^{huGRPr} cell line, as well as verification of the presence, quantitative expression, and biological activity of the Ace-1^{huGRPr}.[15,16] The prior work described the creation and imaging of nude mouse xenografts of this cell line and the Ace-1 parent cell line. IR800-G-Abz4-t-BBN, a human BBN agonist, was synthesized and characterized previously.[14] We will summarize briefly selected methods used in prior work to facilitate a clear understanding of the procedures used in this study.

IR800-G-Abz4-t-BBN is soluble enough in aqueous media for the in vitro cell studies. For arterial delivery, it is formulated in 2 mL (up to 50 μM) by diluting a stock 5 mM DMSO solution 100-fold with phosphate-buffered saline (PBS).

Xenografts of Ace-1^{huGRPr} tumors were grown in nude mice as described. After the tumors reached 0.5–1 cm in diameter, the tumors were excised and minced with a scalpel or razor blade.

To place the catheter at the canine prostatic artery, we used X-ray fluoroscopy guided with an iodinated X-ray contrast agent, iodixanol (Visipaque 320, General Electric Healthcare, Princeton, NJ). To ensure that the highly concentrated (~0.5 M) X-ray agent did not block the binding of IR800-G-Abz4-t-BBN to GRPr, we duplicated our previously published radioligand binding assay, but in the presence of 0–10% iodixanol.[12] Ace-1^{huGRPr} cells were seeded at 30 000 cells per well in a 96-well plate in triplicate. Cell culture medium was replaced 24 h later with 100 μL of binding buffer (RPMI 1640, 20 mM HEPES, 0.1% BSA w/v, 0.5 mM PMSF, and 0.1 mg/mL bacitracin) at room temperature and the plate was then kept at 4°C for 30 min to allow the medium to cool slowly. The buffer was replaced with 60 μL of binding buffer containing a constant concentration of ^{125}I-Tyr^4-BBN (0.22 μCi/mL) (Perkin Elmer) and a range of concentrations (0.1 nM-1 μM) of IR800-G-Abz4-t-BBN.

Binding buffers were made at 0, 1, 5, and 10 mol% iodixanol. After incubation of the binding solutions with the plated cells on ice for 1 h, the cells were washed five times with ice-cold wash buffer (25 mM HEPES, 150 mM NaCl, pH 7.4), and then lysed in 100 μL of 1 N NaOH. Solutions were then transferred to scintillation tubes and the radioactivity was measured using an automatic gamma counter (PerkinElmer Wizard II, Model 2480). The data were analyzed using GraphPad Prism 5 and reported as mean ± SE.

2.3 | Immune suppression of dogs

Orthotopic tumors in dogs were originally reported with the parent Ace-1 cell line implanted into cyclosporine immune-suppressed dogs.[11] Keller et al used oral cyclosporine to achieve trough levels of 400–600 ng/mL. In Dog 1, we attempted to repeat this procedure, implanting Ace-1^{huGRPr} cells into a cyclosporine (Atopica, cyclosporine A, Novartis) immune-suppressed beagle. Cyclosporine was administered (200 mg/d) and blood levels were monitored to ensure that nadir drug concentrations at 24 h after dosing were >400 ng/mL. Since no tumor growth was identified in Dog 1, a more potent immunosuppressive protocol was applied in Dogs 2–6. The starting dose of cyclosporine was increased from 200 to 300 mg/d, and 2.5 mg/kg/2d azathioprine, 1 mg/kg/d prednisolone, and methylprednisolone (Depo-Medrol, Zoetis Animal Health) (1 × 10 mg/kg IM once on the day of implantation) were added to the immunosuppression protocol. The conditions and drug regimen for each animal are shown in Table 1. Nadir blood cyclosporine concentrations (24 h after morning dosing) were 400–1200 ng/mL.

2.4 | Implantation of orthotopic Ace-1^{huGRPr} tumor cells

Cells were harvested into PBS and kept on ice for less than 1 h prior to implantation. Table 1 lists the cell numbers implanted in each dog. Between 20 and 30 million cells were implanted to the prostate parenchyma in five closely geographically spaced injections. Dogs were sedated with dexmedetomidine (10 ug/kg) and butorphanol (0.2 mg/kg) and positioned supine. Using a multifrequency, curvilinear ultrasound transducer (4.2–10.4 MHz, Aplio 300, Toshiba America Medical Systems, Tustin, CA 92 780), the prostate gland was located transabdominally. The canine prostate gland is in the caudal abdomen, caudal to the urinary bladder and cranial to the pubic bone. Using ultrasound guidance, a syringe fit with a 1.5-inch 22-gauge needle was guided into the right or left lobe of the prostate gland. In Dogs 1–3, after injection of the tumor cells, the syringe and needle was simply drawn out. To better restrict extra-prostatic tumor growth, in Dogs 4–6 we sealed the implantation wounds with n-butyl cyanoacrylate (Vetbond, 3M). To minimize exteriorization of the cancer cells, after the tumor cells were injected into the prostate gland, the syringe containing the cancer cells was removed from the needle without withdrawing the needle tip from the interior of the prostate gland, and a second syringe containing the wound sealant was then attached to the needle. Then 50 uL of Vetbond was injected. In Dog 2 we also injected 6×10^6 of Ace-1^{huGRPr} or Ace-1 cells in 1 mL subcutaneously into the dog's flanks to assess tumor growth rates outside of the prostate gland.

2.5 | Ultrasound (US) and magnetic resonance imaging (MRI)

US was used to observe tumor growth beginning at week fo4 following implantation of the tumor cells. Upon detection of an obvious 1–2 cm mass in the prostate gland, the dogs were

imaged with MRI. Under general anesthesia dogs were placed in the supine position. MRI was performed using a 3 Tesla MRI body imager (Achieva for dogs 1 and 2 or Ingenia for dogs 3–6, Philips Healthcare, Cleveland, OH) in combination with an 8-channel (dogs 1 and 2) or 16-channel (dogs 3–6) knee coil. An axial T2 weighted (W) turbo spin echo (TSE) (TE = 110 ms TR = 23.7s, flip angle 90 slice thickness = 3 mm FOV 180 mm) and a pre- and post-contrast axial T1W TSE pre and post-contrast (TE = 10 ms TR = 269 ms Flip angle 90, slice thickness 3 mm FOV = 180 mm) were acquired. A bolus injection of 0.2 mmol/kg gadobenate dimeglumine (MultiHance™, Bracco Diagnostics Inc., Monroe Twp, NJ) was administered before the post-contrast T1W TSE scan via an intravenous catheter placed in the cephalic vein.

2.6 | Angiography and drug delivery

Canine angiography and drug delivery were performed under general anesthesia and sterile conditions according to protocols approved by the Institutional Animal Care and Use Committee. The right carotid artery was surgically accessed and a 6-French vascular sheath was placed. A 5-French selective catheter (Angled Glidecath, Terumo Interventional Systems, Somerset, NJ) was used to select the internal iliac arteries and obtain selective angiograms with iodixanol contrast on DSA (digital subtraction angiography) fluoroscopy. After selective angiography of the internal iliac arteries, the ipsilateral prostatic artery supplying the prostate lobe containing the tumor was selected using a Renegade Hi-Flo microcatheter with a Fathom microwire (Boston Scientific, Natick, MA). Super selective microcatheter DSA from the prostatic artery was performed from multiple projections using iodixanol contrast to confirm catheter positioning. From this position, a 2–3 mL saline flush was delivered to dilute the iodixanol. The 2 mL solution of IR800-G-Abz4-t-BBN (25–100 nmol) was delivered over 2 min. The IR800-G-Abz4-t-BBN delivery was followed by a saline flush of sufficient volume to clear the catheter of the NIRF agent. The agent was allowed to dwell for 60 min (dogs 1 and 2) or 20 min (dogs 3–6), facilitated by leaving the catheter in place with the assumption that the catheter greatly inhibited the arterial blood flow. In dogs 1 and 2, a 2 × 2 mL saline flush was then delivered followed by catheter removal and euthanasia. In dogs 3–6, the catheter was removed after the 20 min dwell time without the final saline flush. The sheath was then removed, the carotid artery ligated, and the skin closed for recovery. Dogs 1 and 2 were euthanatized after the procedure. Dogs 3–6 were euthanized 24 h after the procedure.

2.7 | Optical NIRF imaging

The tissue excision procedure was monitored in real-time using a Fluobeam™ 800 NIR imaging system (Fluoptics, Grenoble, France) equipped with a 780 nm laser (7 mW/cm^2) for excitation and a >820 nm emission filter. Imaging was performed on excised tissues immediately after euthanization. In Dog 3 we also imaged the excised, sectioned prostate gland bearing a large tumor following storage of the tissue for 24 h in formalin to explore the effect of the formalin on the dicyanine fluorophore. Formalin fixation had little effect on the NIRF intensity. The intensity of NIRF from dissected tissues is judged to be only semi-quantitative due to signal attenuation of incident and emitted light that is characteristic of NIRF imaging. We therefore do not report quantitative data.

2.8 | Histopathology

All of the tissues discussed were obtained postmortem, imaged immediately at necropsy, and then preserved in neutral-buffered formalin. The tissues were embedded in paraffin, 4 μm sections were cut and stained with hematoxylin and eosin, and examined 2 by 2 veterinary pathologists (TJR and SME).

3 | RESULTS

In vitro studies. Figure 1 shows the structure of the peptide conjugate and the competition binding curves in the presence of iodixanol, the X-ray contrast agent used to guide the catheterization (Figure 1A). We chose iodixanol for the angiography because it is the only isotonic X-ray contrast agent that is commercially available in the high concentrations that are ideal for the fluoroscopic catheterization guidance. Our rationale was that excessive osmolality might have a significant effect on the biology of the cancer or non-cancer cells that might limit receptor expression or binding of the NIRF agent. We previously demonstrated that Ace-1^{huGRPr}, but not Ace-1 cells expressed huGRPr and bound IR800-G-Abz4-t-BBN with 4 nM IC50 against ^{125}I-Tyr^{4}-BBN. We also demonstrated that the expressed huGRPr was biologically active and internalized IR800-G-Abz4-t-BBN. Iodixanol suppressed some, but tolerable amounts of receptor binding, even when there was 10% iodixanol in the medium (Figure 1B). Binding in a higher iodixanol concentration progressively increased IC50, but only from 8 to 25 nM, and it diminished the apparent receptor concentration by only ~20%. Because these were considered acceptable suppressions, we did not attempt to ascertain the mechanism. In light of these findings we added a saline wash step after catheter placement and before administration of the 2 mL of IR800-G-Abz4-t-BBN.

3.1 | Histopathology

Observations of tumor presence or absence were confirmed in all cases by histopathology using four, H&E-stained, cross-sections of the prostate gland. Grossly, there was mild to moderate enlargement of the prostate gland in all dogs due to expected background benign papillary and/or cystic prostate hyperplasia in adult, intact, male Beagle dogs. Firm tumor nodules were observed and palpated on the prostatic surface in dogs 2–6. On cut section, there were gray/white/yellow subcapsular, intraprostatic, or periurethral tumors (Figure 2) with mild hemorrhage and fibrosis. In dog 1, there were multifocal areas with lymphoplasmacytic inflammation. No neoplasms were detected in dog 1 likely due to immune rejection of tumor growth. In dog 2, Ace-1^{huGRPr} and Ace-1^{CMV} cell lines formed tumors in the prostatic capsule. Ace-1^{huGRPr} neoplastic cells formed large cribriform glands with necrosis and hemorrhagic centers while Ace-1^{CMV} cells formed solid sheets of tumor cells with desmoplasia. Tumors that originated from Ace-1^{huGRPr} cells in dogs 3–6 were poorly demarcated, small to large nodules of prostatic carcinoma that invaded prostatic acini, ducts, and interlobular septae. Prostatic carcinomas were seen in different locations inside the prostate gland. The locations included the center of the prostatic lobe, periurethral area, prostatic capsule and extracapsular regions (Figure 2B-E). Ace-1^{huGRPr} cancer cells grew in variable patterns inside the gland. In most cases, they formed cribriform glands with or without central coagulation necrosis (Figures 2F and 2G) or small irregular cribriform fused

glands with slit-like lumens or alveoli in the center of the nodule (Figure 2H). The neoplastic cells were well to moderately differentiated, large and polygonal with amphiphilic cytoplasm, round to oval enlarged nuclei, and prominent nucleoli. Some neoplastic cells had vacuolated bluish cytoplasm. Some neoplastic cells formed poorly defined lobular patterns that lacked a cribriform architecture and formed an irregular infiltrative basaloid pattern. Most neoplastic cells in the periphery of the tumor nodules showed epithelial to mesenchymal transformation with mucin and tissue infiltration (Figures 2I and 2J). Prostatic cancers originating from Ace-1^{huGRPr} mouse tumor chunks formed cystic cavities lined with pleomorphic anaplastic cells and their lumens were filled with sloughed neoplastic cells and eosinophilic cellular debris (Figures 2K and 2L). Ace-1^{huGRPr} mouse tumor chunks induced lymphoplasmacytic inflammation around and in between the cystic cavities. In all dogs, mild to moderate mononuclear inflammation was present around the tumors that included plasma cells, lymphocytes, and macrophages. In addition, there was variable desmoplasia in and around the prostate tumors. Neoplastic emboli were seen occasionally in dilated subcapsular lymphatics.

The characteristics of Ace-1^{huGRPr} and Ace-1^{CMV} subcutaneous tumors were similar to those that formed in the prostate gland with tumor invasion into skeletal muscle and adipose tissue (Figures 2M and 2N). Mucinous infiltrative prostatic carcinoma was present at the periphery of the tumors. Moderate desmoplasia and multifocal lymphoplasmacytic inflammation were present in the tumors. Lymph node tumor metastasis was seen in dogs 4 and 5 and was characterized by large discrete neoplastic nodules that occupied both cortex and medulla and replaced approximately half of the lymphoid structure (Figure 2O). The neoplastic cells were arranged in a cribriform (Figure 2P) to infiltrative pattern with desmoplasia, necrosis, and hemorrhage. A mucinous infiltrative neoplastic pattern with invasion of lymphatic vessels was also present.

3.2 | Dog prostate imaging studies

Table 1 summarizes the procedural differences among the six dogs. In Dog 1, which grew no tumors, we placed the catheter at the prostatic artery, opened the abdominal cavity under anesthesia, and imaged the living animal as we administered the NIRF agent in aliquots. Our aim was to verify that the concentration of IR800-Abz4-t-BBN was sufficient to visualize in the prostate gland, to estimate the amount of the agent required to perfuse the gland, the volume needed and the initial kinetics. We used a 10 nmol/mL solution in PBS, and initially delivered two 0.2 mL aliquots (4 nmol) at time 0 and 15 min later. The NIRF signal was visible by 15 min. but not immediately upon infusion (Figure 3). The signal was brighter at 30 min. The remaining agent was then administered in two doses 15 min apart, and images in Figure 3 were taken over the next hour with the catheter in place. Perfusion of 2 mL of the NIRF agent into arteries and veins was probably followed by slower diffusion through extracellular spaces, starting deeper within the gland, and diffusing toward the surface of the gland. Somewhat surprisingly, both lobes of the prostate were seen at roughly equal brightness, even though only the left prostatic artery was used for the administration of agent. This suggests a robust collateral circulation in the canine prostate gland. After euthanasia of Dog 1, 2 h after initial injection of the agent, the gland and local tissues were excised and imaged optically (Figure 3E-H). No significant signal was observed in the urine

and blood (not shown), muscle, and fat. The bladder was enhanced but to a lesser degree than the prostate gland. Figure 3F shows that the gland was well, but not evenly perfused, with NIRF signal considerably greater in the center of the gland, and somewhat more signal in the left lobe, the side where the catheter was placed.

For Dog 2, the more robust four-agent immune suppression protocol produced abundant tumors, with an otherwise similar experimental protocol. Both intraprostatic and extracapsular tumors were visible in the NIRF images and in the MRI scanned 24 h before catheterization. Considerable background NIRF was apparent from IR800-G-Abz4-t-BBN that had failed to wash out of the normal prostate areas in the 1 h incubation period, similar to Dog 1. Surprisingly, two implanted flank tumors grew much faster (>10×) than the implanted prostatic tumors, becoming larger even than the whole prostate gland, with cavernous central necrosis.

In Dog 3, we followed the same procedures as for Dog 2, but recovered the animal for 24 h before euthanasia. Figure 4 shows the images for dog 3. US (Figure 4A) was used to determine when tumor growth had reached 1–2 cm. The T1 THRIVE MRI was able to demonstrate extracapsular tumor enhanced with the Gd contrast agent (Figure 4C). The T2W TSE HR T2 image in Figure 4D showed the best separation of prostate from extensive tumor growing abundantly along the needle track from the implantation. Shadowing signal within the prostate gland in this image also indicated the presence of tumor inside the gland. Figure 4B demonstrates with X-ray fluorography, the placement of the catheter (arrow) in the prostatic artery. The photographic and NIRF imaging on the excised structures (Figure 4E-H) demonstrates very high NIRF contrast between the prostate gland and bladder and all other tissues. Imaging the whole prostate gland in Figure 4F also shows very bright cancer nodules on the superficial capsule. A section of the prostate gland is shown along with its corresponding NIRF image in Figures 4G and 4H. The tissue photographs Figures 4E and 4G, and their manually co-registered NIRF images in Figures 4F and 4H, respectively and associated histopathology together demonstrate that the Ace-1^{huGRPr} tumor grew inside the prostate gland and that the intrarterial delivery of IR800-G-Abz4-BBN targeted primarily the cancer and not the BPH present in the adjacent prostate tissue.

Dogs 4–6. In these three dogs we confirmed the repeatability of tumor growth in the model. We added a VetBond seal of each implantation wound to inhibit the growth of extra-prostatic Ace-1^{huGRPr} cells. We also attempted to grow tumors from minced mouse xenografts of Ace-1^{huGRPr} cells, implanting these in the prostate lobe contralateral to the one in which the Ace-1^{huGRPr} cells were implanted. All catheterizations and arterial injections of the NIRF agent were made to the same side of the prostate with the implanted Ace-1^{huGRPr} cells. The Vetbond sealing technique stopped seeding along the implantation track in all three animals. Tumors grew well inside the prostate gland from the implanted Ace-1^{huGRPr} cells, while the xenograft mice tumor material did not grow significantly. Figure 5 shows the MRI and NIRF imaging results for Dog 4 (100 nmol dose of IR800-G-Abz4-t-BBN). There is a powerful NIRF signal in the sectioned excised prostate gland from the tumor (Figure 5C) that was clearly identified on the T2 MRI scans of the living animal prior to catheterization (Figures 5A and 5B). Not seen in the MRI, but extremely bright in the NIRF images was the vas deferens (partially covered by wooden tongue depressors in Figure 5C). This signal was

bright in the NIRF images prior to excision of the gland so it was followed in real time by the necropsy pathologist who located a small (<1 cm) lymph node that glowed faintly under NIRF imaging. Histopathology later confirmed tumor cells in the lymph node and in lymph channels of the prostate gland, suggesting that the tumor cells in the node had seeded through a lymph channel, possibly one that runs along the vas deferens. The brightness of the vas deferens suggests also that some migration of the NIRF agent into the vas deferens occurred from retrograde flow.

We also tested three doses of the NIRF agent, 100, 50, and 25 nmol in Dogs 4, 5, and 6, respectively, to assess the sensitivity for detection of IR800-G-Abz4-BBN with the Fluobeam imager. Figure S1 contains Fluobeam images at different doses and exposure times demonstrating a dose effect for retention of NIRF signal. Qualitatively, we found that 50 nmol was a sufficient arterial dose for NIRF imaging of the growing tumor inside the sectioned prostate gland using the Fluobeam imager at an exposure of 150 ms.

4 | DISCUSSION

An effective pharmaceutical approach to expand the use of AS would preserve prostate gland function in 1000 of men who currently cannot qualify for AS due to the presence of aggressive biomarkers, tumor location, or younger age. Several gland-sparring focal ablation therapies are being explored in support of this goal, for example, thermo- and cryotherapy, photodynamic therapy, and high frequency ultrasound (HIFU).[17–19] These forms of therapy imperfectly estimate the tumor margins and would benefit from subsequent adjuvant therapy provided that it is free of serious side effects. In addition, focal therapies are unlikely to be effective in multifocal disease that is common even in intraglandular localized prostate cancer.

One therapy that is well adapted in this overall context is Peptide Receptor Radionuclide Therapy (PRRT).[20] PRRT uses small (<2 kDa) peptides conjugated to powerful alpha and beta emitting isotopes (eg, ^{177}Lu-DOTAtate, ^{177}Lu-AMBA) as anti-cancer therapeutics. The peptides have nM affinity for hormone receptors overexpressed on various cancers. The prominent hormone receptor-peptide combinations tested in humans are somatostatin (SST) and gastrin-releasing peptide receptors (GRPR), as ^{68}Ga-peptide PET imaging agents and ^{177}Lu-peptide PRRT agents.[21,22] While the off-target radiation toxicity of systemically administered PRRT agents would be too great to treat early stage prostate cancer patients, we hypothesize that the off-target effects will be minimal to nonexistent if the agents can be effectively delivered intra-arterially to the prostate gland at a small fraction of the systemic dose. Our canine model of prostate cancer is being developed to test the hypothesis that PRRT will be useful in this therapeutic context.

We believe our study represents the first time a human cancer growth factor receptor has been expressed and grown in an experimental dog model of prostate cancer. Starting with a known isolated Ace-1 canine prostate cancer cell line that expresses very little mRNA for GRPr and does not bind GRPr targeting peptides, our prior study demonstrated that the Ace-1 cell line could be transfected with human GRPr. The resulting Ace-1^{huGRPr} cells expressed the GRPr receptor on their surfaces and the receptor functioned biologically as a

growth factor, grew reliably in nude mice, and could be optically imaged in vivo and microscopically with IR800-G-Abz4-t-BBN.[12–14] The histopathology results reported herein definitively demonstrate the growth of these cells in the prostate glands and other tissues of immunosuppressed dogs, as well as the cells' ability to seed to regional lymph nodes. The new canine model reported herein is thus the first time a human cancer growth factor expressing cell has been grown in dogs.

Fluorescent NIRF imaging data are not reliably quantitative due to high attenuation of the NIRF signal by tissue. However, the data are sufficiently strong to establish useful facts and validate our model for use in studies using imaging and therapeutic human GRPr-targeted agents, which we are now doing, testing PRRT delivered intra-arterially. Notably, IR800-G-Abz4-t-BBN was silent in BPH that would otherwise provide a significant noncancerous target tissue in our therapeutic scheme. We also verified in separate control dogs without tumor cell implantations that no NIRF signal was present without administration of the NIRF agent, and that 100 nmol of arterially administered NIRF agent dispersed and was barely detectable after 24 h at the normal image exposure times (~100 ms) used to image the tumor implanted in dogs.

The catheterization has been performed in about 20 min by two experienced interventional radiologists, who consistently reached the gland surface. The canine prostate gland was remarkably well perfused, so that a similar signal was seen in both lobes of the gland from administration into only one lobe via the right or left prostatic artery. The NIRF agent was bright enough to image tumor cells in the sectioned gland that were growing within the gland from the central region close to the urethra, out to the subcasular and capsular regions. We were furthermore able to track the migration of the cancer cells within a lymph channel to a deeply buried small lymph node that was imaged with NIRF contrast from outside of the node, with pathological confirmation of tumor cell deposits in the node. Our initial dose of 100 nmol into the ~35 g prostate was easily detected, and the threshold for detection of tumor ex vivo in a sectioned prostate gland with our imager in a darkened room appeared to be about 50 nmol in the concentration series. Mice weighing 25 g bearing subcutaneous 0.5–1.0 g Ace-^{1huGRPr} tumors are imaged using IR800-G-Abz4-t-BBN administered intravenously at 10 nmol (10 nmol/0.025 kg) for a 1 g tumor, similar in size to the canine tumors (50–100 nmol/0.035 kg). The difference is probably attributable to the more efficient exposure of the tumor to the agent in mice which typically establish angiogenesis, compared to the situation in these dogs, where histopathology indicated a more multifocal growth pattern.

Cyclosporine alone sufficed in the initial development of the model by Keller et al[11] (12). Human cancer cells do not grow consistently in cyclosporine immune-suppressed dogs due to residual immune capability, but the Ace-1 canine prostate cancer cell line[23–25] was exceptional. In the study of Keller et al, 40% of the dogs had tumor in the capsule and 60% had tumor in the prostate interior. Fifty percent of animals also developed metastases, mainly in lymph nodes. Compared to the previous dog study using the Ace-1 cells, the present work required significantly more effective immune suppression of the dogs. GRPr is a highly species homologous protein, but the human GRPr on the surface of the canine Ace-1 cells likely exposed the dogs to human antigens. In addition, the transfectant

contained HIS tags. When the initial dog on cyclosporine alone failed to develop tumors we initiated the 4-drug regimen as described, which was successful in allowing tumors to grow quickly. The side effects of the extra immune suppression drugs were obvious in Dog 5; however, which developed a bacterial infection of his foot that required treatment with systemic antibiotics. In addition, the dog was too weak to undergo the anesthesia for MRI at week 6. Short term studies of up to 6 weeks would probably be readily tolerated by most dogs with the enhanced immune-suppression, but months long therapeutic studies could be problematic. Elimination of the human fragments in the huGRPr vectors should allow use of cyclosporine alone to suppress the immune system, which we expect will allow a 4–6 month therapeutic regimen to be tested.

The fact that the Ace-1 canine prostate cancer cells grow readily in immune-suppressed dogs will allow us to test GRPr-specific imaging and therapy drug candidates in a large animal model whose prostate gland is approximately the same size as in man, and within which BPH is predominant. The ability to transfect the Ace-1 cell line with human receptors makes it a promising candidate cell line for research screening on further variants containing the other GRPR subtypes, such as the NMBR expressed in human prostate cancer, and the BB3 subtype found in human pancreas,[26] as well as for screening other human receptors potentially useful in prostate cancer therapy, such as PMSA.[27]

5 | CONCLUSIONS

A human receptor expressing cell line has been for the first time grown within the prostate gland of dogs. Ace-1^{huGRPr} expressing tumors and cells grow readily when implanted in the canine prostate gland of immune-suppressed, middle-aged beagles. The cells grow outside the prostate as well, and at an extraordinarily rapid rate. The model expresses a validated human growth receptor, GRPr, which maintains its activity for a known binding ligand, and metastasizes to local lymph nodes. A useful model option is to use super selective catheterization of one canine prostatic artery to deliver exogenous agents to both prostate lobes in high concentrations, but very low overall doses. GRPr receptor expressed on the tumor cells remains functional in vivo. Together with a published mice dual tumor Ace-1/Ace-1^{huGRPr} screening model, the system provides a rapid semi-quantitative estimate of specific to nonspecific binding of new GRPr specific agents in mice followed by rapid scale up to an analogous dog model. We envision testing of various novel focal prostate cancer therapies, as well as creation of models expressing other useful human receptors.

Supplementary Material

Refer to Web version on PubMed Central for supplementary material.

ACKNOWLEDGMENTS

MFT wishes to acknowledge The Stefanie Spielman Foundation. MFT, TR, and MVK thank the James Comprehensive Cancer Center for a Pelotonia pilot grant. We acknowledge NIH NIBIB 1 R01 EB022134 and P30 CA016058 for financial support. The Ohio State College of Veterinary Medicine Biospecimen Repository was supported by the following grants: UL1TR001070 from the National Center for Advancing Translational Sciences. All of the work was supported by P30CA016058 from the National Cancer Institute to The Ohio State University. We acknowledge support from the College of Veterinary Medicine Canine Research Funds.

Funding information

National Center for Advancing Translational Sciences, Grant number: UL1TR001070; National Cancer Institute, Grant number: P30CA016058; College of Veterinary Medicine Canine Research Funds; National Institutes of Health, Grant numbers: 1 R01 EB022134, P30CA016058; James Comprehensive Cancer Center

REFERENCES

1. Filson CP, Natarajan S, Margolis DJA, et al. Prostate cancer detection with magnetic resonance-ultrasound fusion biopsy: the role of systematic and targeted biopsies. Cancer 2016;122:884–892. [PubMed: 26749141]
2. Ross AE, D'Amico AV, Freedland SJ. Which, when and why? Rational use of tissue-based molecular testing in localized prostate cancer. Prostate Cancer Prostatic Dis 2016;19:1–6. [PubMed: 26123120]
3. Sauter G, Steurer S, Clauditz TS, et al. Clinical Utility of Quantitative Gleason Grading in Prostate Biopsies and Prostatectomy Specimens. Eur Urol 2016;69:592–598. [PubMed: 26542947]
4. Network NCC. NCCN Clinical Practice Guidelines in Oncology Prostate Cancer V22017 2017 [Available from: https://www.nccn.org/professionals/physician_gls/pdf/prostate.pdf.
5. Tosoian JJ, Carter HB, Lepor A, Loeb S. Active surveillance for prostate cancer: current evidence and contemporary state of practice. Nature Reviews Urology 2016;13:205–215. [PubMed: 26954332]
6. Pollack A, Zagars GK, Starkschall G, et al. Prostate cancer radiation dose response: Results of the M. D. Anderson phase III randomized trial. Int J Radiat Oncol Biol Phys 2002;53:1097–1105. [PubMed: 12128107]
7. Liapi E, Geschwind JF. Transcatheter and ablative therapeutic approaches for solid malignancies. J Clin Oncol 2007;25:978–986. [PubMed: 17350947]
8. Marelli L, Stigliano R, Triantos C, et al. Transarterial therapy for hepatocellular carcinoma: Which technique is more effective? A systematic review of cohort and randomized studies. Cardiovasc Intervent Radiol 2007;30:6–25. [PubMed: 17103105]
9. Kaplan SA. Prostate Arterial Embolization is a Viable Option for Treating Symptoms of Benign Prostatic Hyperplasia. J Urol 2017;198: 9–10.
10. Gao YA, Huang Y, Zhang R, et al. Benign prostatic hyperplasia: prostatic arterial embolization versus transurethral resection of the prostate–a prospective, randomized, and controlled clinical trial. Radiology 2014;270:920–928. [PubMed: 24475799]
11. Keller JM, Schade GR, Ives K, et al. A novel canine model for prostate cancer. Prostate 2013;73:952–959. [PubMed: 23335024]
12. Ding HM, Kothandaraman S, Gong L, et al. A human GRPr-Transfected ace-1 canine prostate cancer model in mice. Prostate 2016;76:783–795. [PubMed: 26940014]
13. Elshafae SM, Hassan BB, Supsavhad W, et al. Gastrin-Releasing peptide receptor (GRPr) promotes EMT, growth, and invasion in canine prostate cancer. Prostate 2016;76:796–809. [PubMed: 26939805]
14. Shrivastava A, Ding HM, Kothandaraman S, et al. A high-Affinity near-Infrared fluorescent probe to target bombesin receptors. Mol Imaging Biol 2014;16:661–669. [PubMed: 24604209]
15. Ding H, Kothandaraman S, Gong L, et al. A human GRPr-transfected Ace-1 canine prostate cancer model in mice. Prostate 2016;76:783–795. [PubMed: 26940014]
16. Elshafae SM, Hassan B, Supsavhad W, et al. Gastrin-Releasing peptide receptor (GRPR) induces EMT, growth, and invasion in canine prostate cancer. Prostate 2016;76:796–809. [PubMed: 26939805]
17. Polascik TJ. Focal therapy of prostate cancer: making steady progress toward a first-line image-guided treatment modality. Curr Opin Urol 2015;25:183–184. [PubMed: 25775366]
18. Muller BG, van den Bos W, Brausi M, et al. Follow-up modalities in focal therapy for prostate cancer: results from a Delphi consensus project. World J Urol 2015;33:1503–1509. [PubMed: 25559111]

19. Muller BG, van den Bos W, Pinto PA, de la Rosette JJ. Imaging modalities in focal therapy: patient selection, treatment guidance, and follow-up. Curr Opin Urol 2014;24:218–224. [PubMed: 24637316]

20. Reubi JC, Macke HR, Krenning EP. Candidates for peptide receptor radiotherapy today and in the future. J Nucl Med 2005;46:67S–75S. [PubMed: 15653654]

21. Reynolds TS, Bandari RP, Jiang Z, Smith CJ. Lutetium-177 labeled bombesin peptides for radionuclide therapy. Curr Radiopharm 2016;9:33–43. [PubMed: 25771366]

22. Hamiditabar M, Ali M, Roys J, et al. Peptide receptor radionuclide therapy with 177Lu-Octreotate in patients with somatostatin receptor expressing neuroendocrine tumors: six years' assessment. Clin Nucl Med 2017;42:436–443. [PubMed: 28263217]

23. LeRoy BE, Thudi NK, Nadella MV, et al. New bone formation and osteolysis by a metastatic, highly invasive canine prostate carcinoma xenograft. Prostate 2006;66:1213–1222. [PubMed: 16683269]

24. Thudi NK, Martin CK, Murahari S, et al. Dickkopf-1 (DKK-1) stimulated prostate cancer growth and metastasis and inhibited bone formation in osteoblastic bone metastases. Prostate 2011;71:615–625. [PubMed: 20957670]

25. Thudi NK, Martin CK, Nadella MVP, et al. Zoledronic acid decreased osteolysis but not bone metastasis in a nude mouse model of canine prostate cancer with mixed bone lesions. Prostate 2008;68: 1116–1125. [PubMed: 18461562]

26. Fathi Z, Corjay MH, Shapira H, et al. Brs-3 − a novel bombesin receptor subtype selectively expressed in testis and lung-Carcinoma cells. J Biol Chem 1993;268:5979–5984. [PubMed: 8383682]

27. Afshar-Oromieh A, Avtzi E, Giesel FL, et al. The diagnostic value of PET/CT imaging with the Ga-68-labelled PSMA ligand HBED-CC in the diagnosis of recurrent prostate cancer. Eur J Nucl Med Mol Imaging 2015;42:197–209. [PubMed: 25411132]

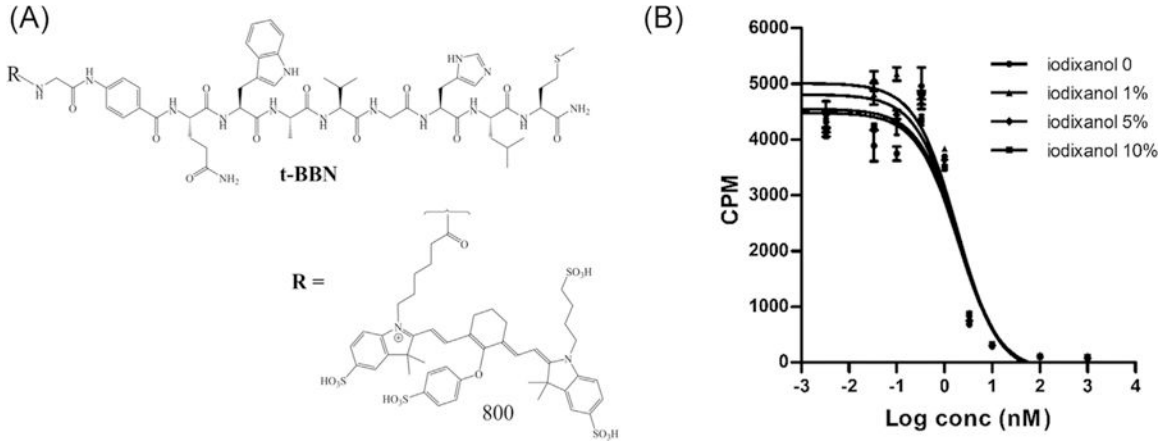

FIGURE 1.

A, Chemical structure of IR800-G-Abz4-t-BBN. B, The effect of the X-ray contrast agent, iodixanol, on IR800-G-Abz4-t-BBN binding to GRPr expressed naturally on the human prostate cancer cell line, PC-3, determined using a competition binding assay against the universal GRPR ligand, ^{125}I-Tyr4-BBN

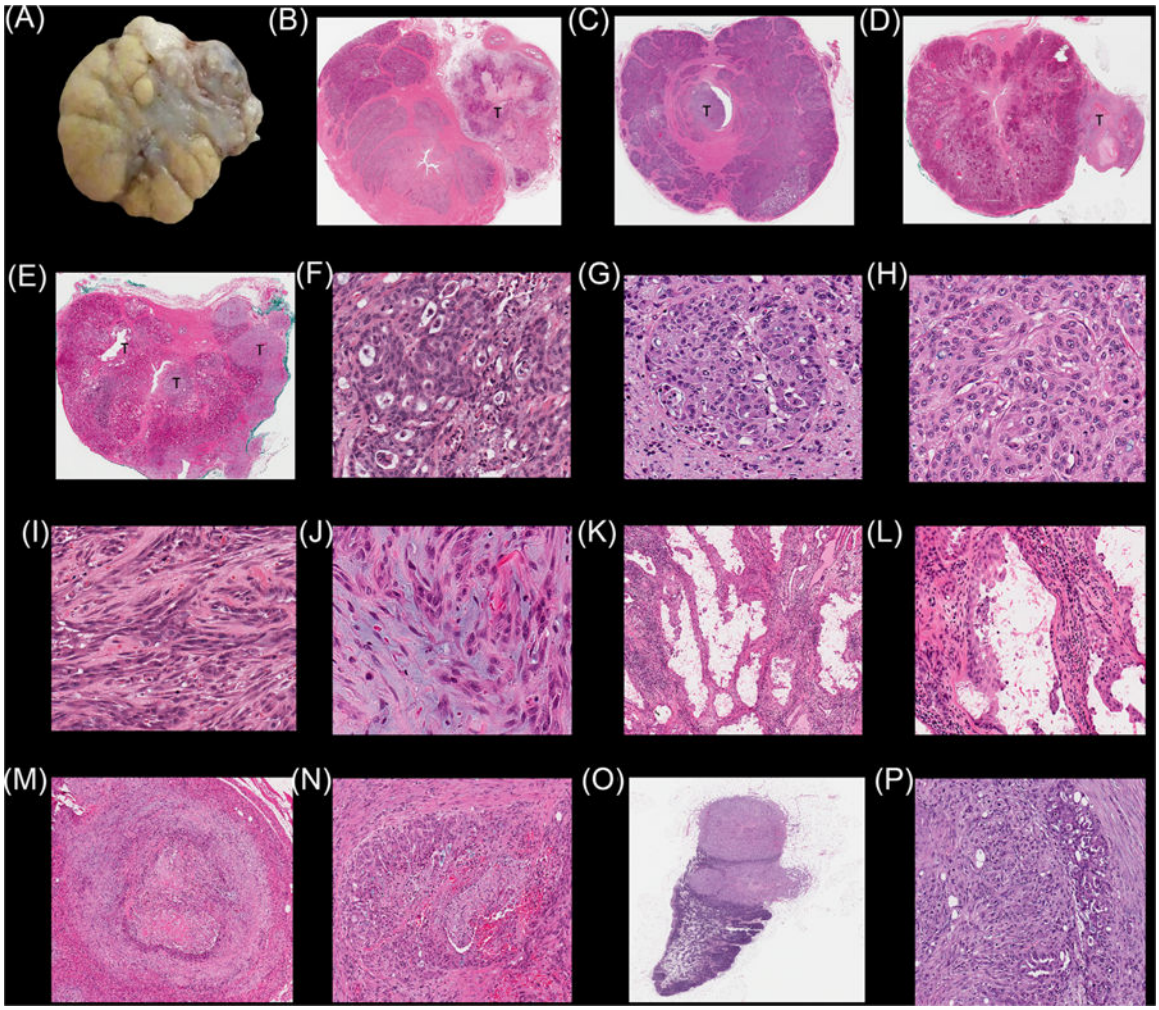

FIGURE 2.

Macroscopic and microscopic characteristics of Ace-1 prostatic tumors and metastases in dogs 3–6 implanted orthotopically and subcutaneously with Ace-1^{huGRPr} prostate cancer cells and mouse Ace-1 xenograft tumor tissue. A, Gross appearance of Ace-1^{huGRPr} prostatic tumor (greyish white area) in dog 3. B-E, Histopathology of the entire prostate glands of dogs 3–6 showing the different sites (periurethral, subcapsular, capsular, and extracapsular) of Ace-1^{huGRPr}-induced prostatic cancers. F-H, Higher magnification of the Ace-1^{huGRPr} prostatic carcinomas showing regular and irregular cribriform growth patterns. I and J, Ace-1^{huGRPr} neoplastic cells exhibit epithelial to mesenchymal properties with production of mucin (J). K and L, Low and high magnifications of Ace-1^{huGRPr} xenografts grown in nude mice. M and N, Histologic appearance of Ace-1^{huGRPr} subcutaneous tumors showing a cribriform growth pattern of neoplastic cells with central necrosis, hemorrhage, and desmoplasia. O and P, Histopathological appearance of lymph node metastases with Ace-1^{huGRPr} tumors in the cortex and medulla and arranged in fused cribriform patterns. [Color figure can be viewed at wileyonlinelibrary.com]

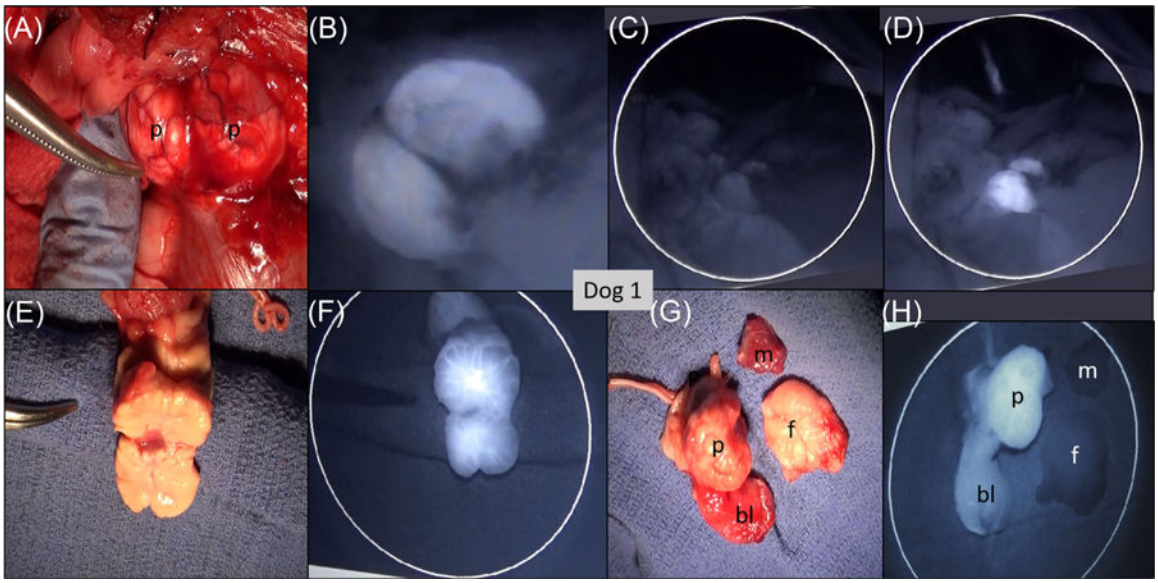

FIGURE 3.

Images of Dog 1. No tumor was present; 24 nmol IR800-G-Abz4-t-BBN was injected into the prostatic artery 1–2 h prior to NIRF imaging in the live dog followed by euthanasia and tissue excision. A, Photograph of the imaging/resection field: P = 2-lobed prostate gland; B, NIRF image of the prostate gland 1 h post administration of the agent. C, NIRF image with the excitation laser turned off. D, Same region as (C) with the excitation laser turned on. Both lobes of the prostate gland were perfused with the NIRF agent from the one-sided arterial administration. E, Photograph of the excised, single sectioned prostate gland, with left lobe on the side of the forceps. F, NIRF image matching photograph in for example, Photograph of the excised specimens: p = prostate, bl = apex of the bladder, m = muscle, and f = fat. H, NIRF image of the same specimens as (G) showing only prostate and bladder with strong NIRF signal. [Color figure can be viewed at wileyonlinelibrary.com]

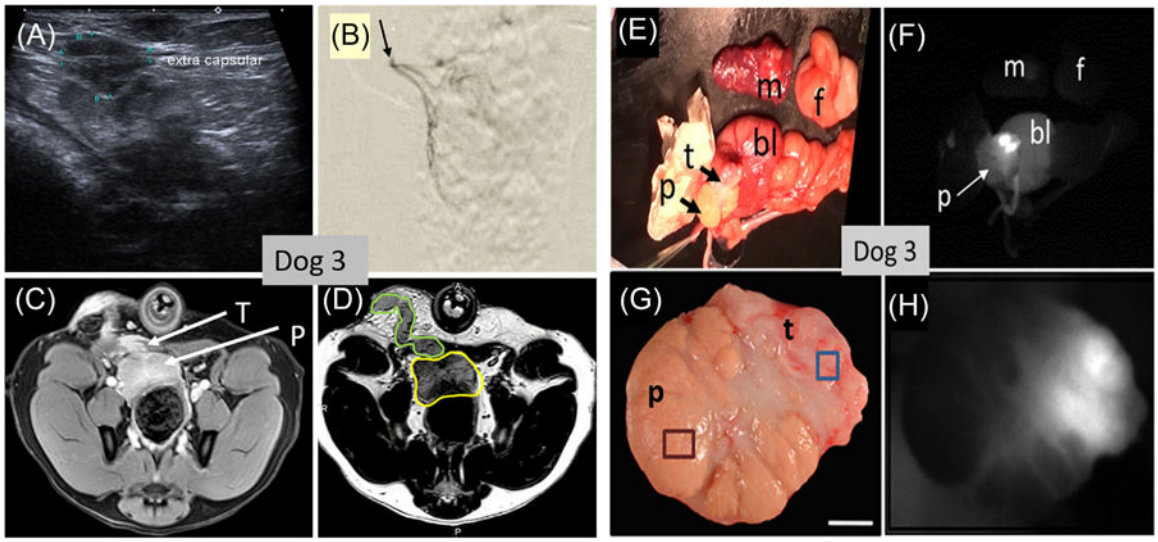

FIGURE 4.

Images of the live dog (A-D) and excised specimens (E-H) of dog 3. A, US image in vivo at week 4 showing heterogeneous (apparent tumor) inside the prostate gland (outline marked green) and apparent extracapsular tumor. B, DSA arteriogram (X-ray fluorography) demonstrating the catheter tip at the prostatic artery. C, T1-weighted MRI scan displaying the prostate gland (p) and extracapsular tumor (t). D, T2-weighted MRI scan with prostate gland outlined in yellow and extracapsular tumor outline in green growing along the implantation needle track. Images (E-H) were taken after 100 nmol of IR800-G-Abz4-t-BBN was injected into the prostatic artery, followed by 24 h recovery, euthanasia, and excision of tissues. (E) photograph and (F) corresponding NIRF image of the excised tissues (abbreviations p = prostate; t = tumor; bl = bladder; m = muscle; f = fat.). G, photograph and (H) NIRF image of a section through the prostate gland showing white NIRF signal only in the tumor-containing region of the prostate gland. Histology showed BPH (brown square region) in the gland not targeted with the NIRF agent and Ace-1 prostate cancer (blue square region) targeted by the NIRF agent. [Color figure can be viewed at wileyonlinelibrary.com]

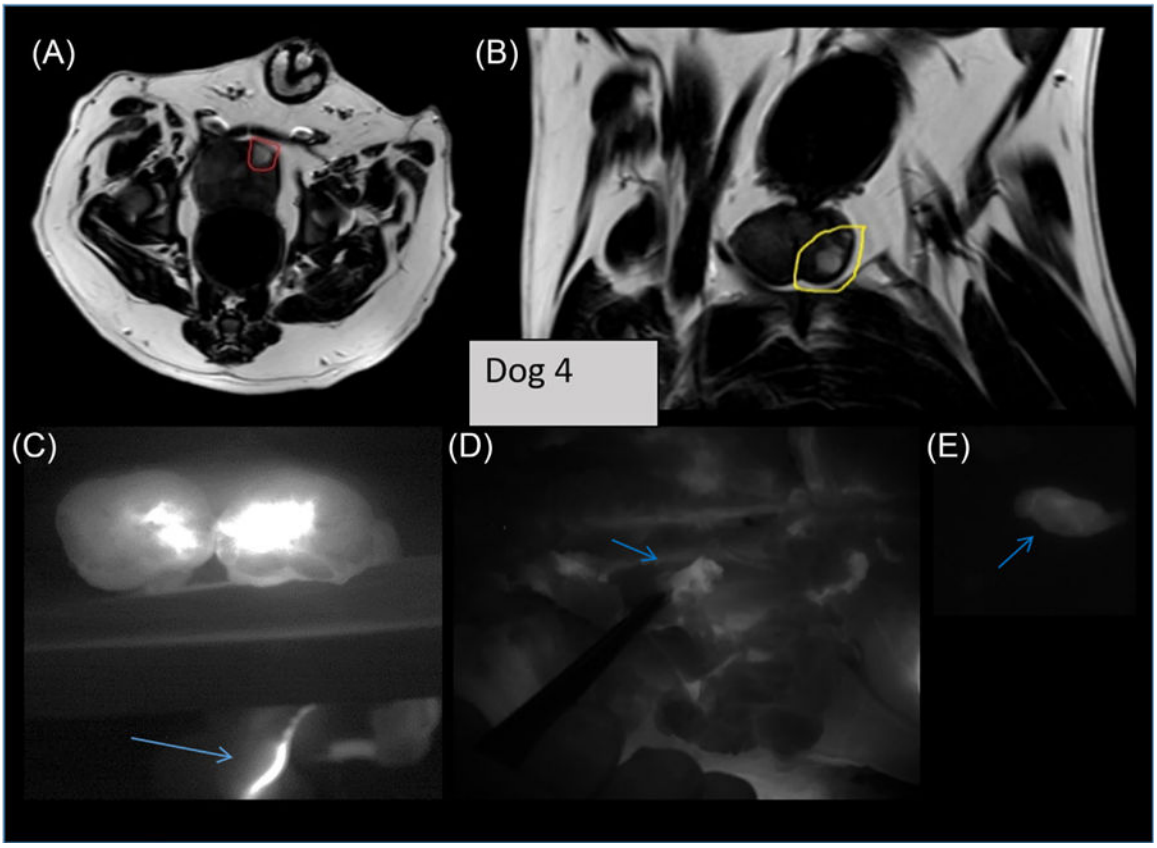

FIGURE 5.

Imaging of dog 4. 100 nmol of IR800-G-Abz4-t-BBN was injected into the prostatic artery, followed by 24 h recovery and excision of tissues. (A and B) are axial and sagittal T2 MRI of the live dog showing the tumor (circled red and yellow) inside of the prostate gland. C, shows the NIRF image of the tumor in the excised, sectioned prostate gland as bright white signal with an arrow pointing to bright area along the vas deferens. D, shows an NIRF image of a slightly enhanced local lymph node, excised and imaged separately in (E) Pathology confirmed tumor cells in the excised lymph node and lymph channels along the vas deferens. [Color figure can be viewed at wileyonlinelibrary.com]

TABLE 1

Experimental details of Ace-1^{huGRPr} implanted dogs

	Dog 1	Dog 2	Dog 3	Dog 4	Dog 5	Dog 6
Weight (kg)	11	12.5	14	10.6	10.1	10.2
Age, Y & M	4 Y	3 Y 4 M	5 Y	3 Y 7 M	5 Y 6 M	6 Y 1 M
Immuno-suppression	1 agent	4 agents	4 agents	4 agents	4 agents	4 agents
Cyclosporine (mg/day)	200	300	300	300	300	300
Nadir Cyclosporine (ng/mL blood)	388	1197	628	1110	805	>400
Cells and implantation sites	huGRPr: 5 × 6 M	Lt: huGRPr 5 × 6 M / 0.1 mL Rt: CMV[a]: 5 × 6 M/0.1 mL	Lt: huGRPr: 5 × 6 M	Rt: huGRPR: 20 M/0.1 mL	Lt: huGRPr: 20 M/0.1 mL	Lt: huGRPr: 20 M/0.1 mL
Chopped mice tumor[b]	None	None	None	Left 0.1 mL	Right 0.1 mL	Right 0.1 mL
SQ implants	None	Lt: huGRPr (60M/1 mL) Rt: CMV[a] (60M/1 mL)	None	None	None	None
Implantation wound Seal	None	None	None	VetBond (0.05 mL, both sides)	VetBond (0.05 mL, both sides)	VetBond (0.05 mL, both sides)
IR800-G-Abz4-t-BBN Dose, nmol in 2 mL	24	100	100	100	50	25
Incubation of agent	1 h	1 h	20 min	20 min	20 min	20 min
Euthanasia, post dose	1 h	1 h	24 h	24 h	24 h	24 h

[a] Ace-1^{CMV} cells are vector transfected cells not expressing huGRPr.

[b] Ace-1^{huGRPr} tumors grown in nude mice excised, finely chopped with a knife, and slurried in 0.1 mL PBS.